Electrical Properties and Dielectric Characteristics CCT-doped Zn/Pr-based Varistors with Sintering Temperature

Choon-Woo Nahm*
Semiconductor Ceramics Lab., Department of Electrical Engineering, Dongeui University, 995 Eomgwangno, Busanjin-gu, Busan 614-714, Republic of Korea

(Received April 9 2009, Accepted June 18 2009)

The microstructure, voltage-current, capacitance-voltage, and dielectric characteristics of CCT doped Zn/Pr-based varistors were investigated at different sintering temperatures. As the sintering temperature increased, the average grain size increased from 4.3 to 5.1 μm and the sintered density was saturated at 5.81 $g \cdot cm^{-3}$. As the sintering temperature increased, the breakdown field decreased from 7,532 to 5,882 $V \cdot cm^{-1}$ and the nonlinear coefficient decreased from 46 to 34. As the sintering temperature increased, the donor density, density of interface states, and barrier height decreased in the range of $(9.06\text{-}7.24)\times10^{17}$ cm^{-3}, $(3.05\text{-}2.56)\times10^{12}$ cm^{-2}, and 1.1-0.95 eV, respectively. The dielectric constant exhibited relatively low value in the range of 529.1-610.3, whereas the tanδ exhibited a high value in the range of 0.0910-0.1053.

Keywords: Microstructure, Sintering, Electrical properties, Dielectric phenomena, Varistors

1. INTRODUCTION

Zinc oxide varistor is a II-VI nonstoichiometric semiconductor device, which the current flowing through it nonlinearly increases with the increase of voltage. Zinc oxide without impurity doping intentionally exhibits ohmic properties at any sintering condition, whereas the zinc oxide doped with minor metal oxides exhibits non-ohmic properties, which leads to the decrease of impedance with increasing voltage.

This nonlinearity of voltage-current properties is due to the presence of a double Schottky barrier formed at the active grain boundaries containing many trap states. Owing to highly nonlinear properties, zinc oxide varistors are used widely in the field of overvoltage protection systems for electric and electronic systems[1,2]. Commercial zinc oxide varistors are generally divided into two categories (called Bi-based and Pr-based ceramics) in terms of oxide inducing inherently nonlinearity. Bi-based zinc oxide varistors have been studied in different aspects since the discovery of zinc oxide non-ohmic ceramics. Although Bi-based zinc oxide varistors show good nonlinear properties, Bi_2O_3 easily reacts with some metals used in preparing multilayer chip nonlinear varistors, and it destroys the multilayer structure[3]. In addition, it is reported to have an additional insulating spinel phase, which does not play a role in electrical conduction[3]. Pr-based zinc oxide varistors have been studied in order to improve a few drawbacks[3], associated with Bi_2O_3[4-15].

To overcome these problems and to obtain the high performance, it is important to comprehend the effect of additives-doping and sintering process on varistor properties[7-15].

The sintering effect on microstructure, electrical properties, and dielectric characteristics of Pr-Co-Cr-Tb-doped zinc oxide varistors was investigated and new some results were obtained.

*Author to whom corresponding should be addressed: electronic mail: cwnahm@deu.ac.kr

2. EXPEIMENTAL PROCEDURE

2.1 Sample preparation

Reagent-grade raw materials were used in proportions of (97.25) mol% ZnO, 0.5 mol% Pr_6O_{11}, 1.0 mol% CoO, 0.5 mol% Cr_2O_3, 0.75 mol% Tb_4O_7. Raw materials were mixed by ball milling with zirconia balls and acetone in a polypropylene bottle for 24 h. The mixture was dried at 120 °C for 12 h and calcined in air at 750 °C for 2 h. The calcined mixture was pulverized using an agate mortar/pestle and after 2 wt% polyvinyl alcohol (PVA) binder addition, granulated by sieving with a 100-mesh screen to produce starting powder. The powder was uniaxially pressed into discs of 10 mm in diameter and 2 mm in thickness at a pressure of 800 $kg \cdot cm^{-2}$. The discs were covered with raw powder in an alumina crucible, sintered at three fixed sintering temperatures (1300 °C, 1330 °C, and 1350 °C) in air for 1 h. The sintered samples were lapped and polished to 1.0 mm thickness. The samples were about 8 mm in diameter and 1.0 mm in thickness. Silver paste was coated on both faces of the samples and ohmic contact of electrodes was formed by heating at 600 °C for 10 min. The electrodes were 5 mm in diameter.

2.2 Microstructure examination

Both surfaces of the samples were lapped and ground with SiC paper and polished with 0.3 μm-Al_2O_3 powder to a mirror-like surface. The polished samples were thermally etched at 1100 °C for 30 min. The surface of the samples was metallized with a thin coating of Au to reduce charging effects and to improve the resolution of the image. The surface microstructure was examined by a scanning electron microscope (SEM) (Hitachi S2400, Japan). The average grain size (d) was determined by the lineal intercept method as follows:

$$d = \frac{1.56L}{MN} \quad (1)$$

where L is the random line length on the micrograph, M is the magnification of the micrograph, and N is the number of the grain boundaries intercepted by the lines[15]. The crystalline phases were identified by an X-ray diffractometry (XRD) (Rigaku D/max 2100, Japan) with Ni filtered CuK_α radiation. The sintered density (ρ) of ceramics was measured by the Archimedes method.

2.3 Electrical measurement

The E-J characteristics of the samples were measured using a high voltage source measure unit (Keithley 237). The breakdown field ($E_{1\ mA}$) was measured at a current density of 1.0 mA·cm^{-2} and the leakage current (J_L) was measured at 0.80 $E_{1\ mA}$. In addition, the nonlinear coefficient (α) was determined from the following expression.

$$\alpha = \frac{\log J_2 - \log J_1}{\log E_2 - \log E_1} \tag{2}$$

where J_1= 1.0 mA·cm^{-2}, J_2= 10 mA·cm^{-2}, and E_1 and E_2 are the electric fields corresponding to J_1 and J_2, respectively.

The capacitance-voltage (C-V) characteristics of the samples were measured at 1 kHz using an RLC meter (QuadTech 7600) and an electrometer (Keithley 617). The donor concentration (N_d) and the barrier height (ϕ_b) were determined by the equation as follows[16]:

$$\left(\frac{1}{C_b} - \frac{1}{C_{bo}}\right)^2 = \frac{2(\Phi_b + V_{gb})}{q\varepsilon N_d} \tag{3}$$

where C_b is the capacitance per unit area of a grain boundary, C_{bo} is the value of C_b when V_{gb}=0, V_{gb} is the applied voltage per grain boundary, q is the electronic charge, and ε is the permittivity of ZnO (ε=8.5ε_o). The density of interface states (N_t) at the grain boundary was determined by the following equation[16]:

$$N_t = \left(\frac{2\varepsilon N_d \Phi_b}{q}\right)^{1/2} \tag{4}$$

The depletion layer width (t) of the either side at the grain boundaries was determined by the following equation[17]:

$$N_d \cdot t = N_t \tag{5}$$

The dielectric characteristics such as dielectric constant (ε_{APP}') and dissipation factor (tanδ) of the samples were investigated in the range of 100 Hz-2 MHz.

Five samples (sintered at the same sintering temperature) were used for all electrical measurements and the average value is presented.

3. RESULTS AND DISCUSSION

Figure 1 shows the SEM images of the samples for different sintering temperatures. The grains uniformly distribute through the entire bulk. The microstructure consisted of primary phase ZnO grain (blackish), and intergranular layer as a secondary phase (whitish), which are a Pr- rich and Tb-rich phases as determined by XRD analysis, as shown in Fig. 2. Added Pr_6O_{11} and Tb_4O_7 were segregated to grain boundaries and nodal points, Pr-oxide and Tb-oxide were found to coexist in the grain boundaries and the nodal points as if they were a single phase.

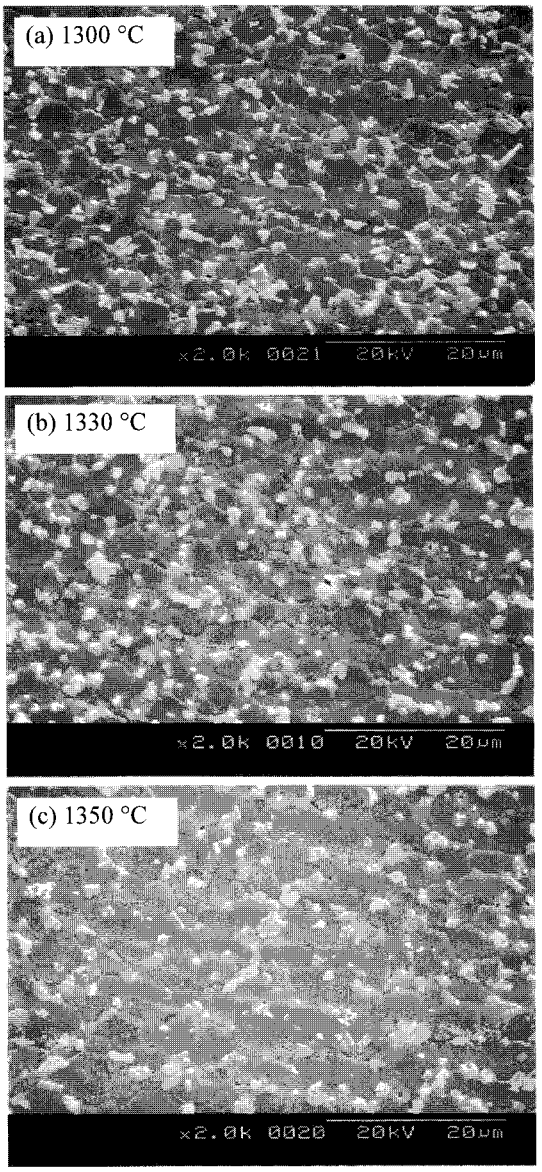

Fig. 1. SEM images of the samples for different sintering temperatures.

The sintered density negligibly increased in the range of 5.81 to 5.82 g·cm^{-3}, whereas it was saturated at nearly 5.81 g·cm^{-3}. It shows very high density so that there is no porosity through the surface microstructure. Nonlinear electro-ceramics added with a few rare earth oxides (REO) don't provide a high sintered density and a high nonlinearity[9-12]. Therefore, the high sintered density is very important for the varistors for high energy capability. The average grain size was linearly increased from 4.3 to 5.1 μm and it was saturated at nearly 5.0 at sintering temperature beyond 1330 °C. The detailed microstructure parameters are summarized in Table 1.

Table 1. Microstructure, V-I, and C-V characteristic parameters of the samples for different sintering temperatures.

Sintering temp. (°C)	d (μm)	ρ ($g \cdot cm^{-3}$)	$E_{1\,mA}$ ($V \cdot cm^{-1}$)	v_{gb} ($V \cdot gb^{-1}$)	α	J_L ($\mu A \cdot cm^{-2}$)	N_d ($10^{17} cm^{-3}$)	N_t ($10^{12} cm^{-2}$)	Φ_b (eV)	t (nm)
1300	4.3	5.81	7,531	3.23	46	9.5	9.06	3.06	1.10	33.7
1330	5.0	5.81	6,411	3.21	44	7.2	7.90	2.72	1.00	34.5
1350	5.1	5.82	5,882	3.02	36	8.4	7.24	2.56	0.95	35.4

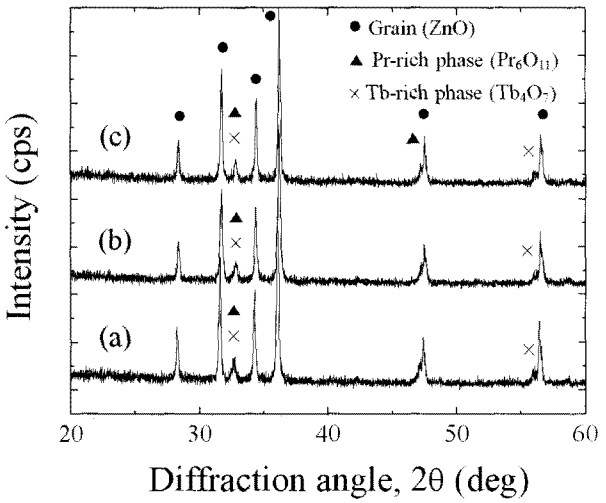

Fig. 2. XRD patterns of the samples for different sintering temperatures; (a) 1300 °C, (b) 1330 °C, and 1350 °C.

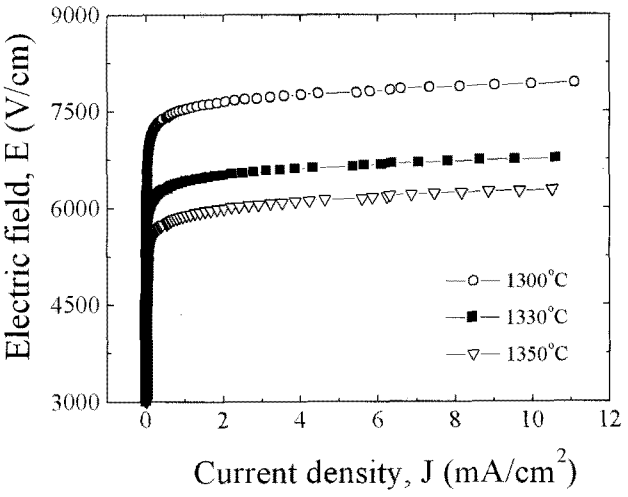

Fig. 3. E-J characteristics of the samples for different sintering temperatures.

Figure 3 shows the E-J characteristics of the samples for different sintering temperatures. The curves show that the conduction characteristics divide into two regions. First, the current does not nearly flow with an increasing field before the critical field (called a breakdown field). Second, the current abruptly increases with increasing electric filed after the critical field (called a breakdown field). On the whole, voltage-current relation is nonlinear. The sharper the knee of the curves between the two regions (which determine the nonlinear coefficient), the better the nonlinear properties. The detailed electrical parameters are summarized in Table 1.

The breakdown field ($E_{1\,mA}$) decreased from 7,531 to 5,882 $V \cdot cm^{-1}$ with the increase of the sintering temperature. All the samples provide a very high varistor voltage per unit thickness (1 mm). This is very important for high voltage nonlinear ceramics with a compact size. The decrease of $E_{1\,mA}$ with increasing sintering temperature can be explained by the grain size and the voltage per grain boundaries. The increase in the number of grain boundaries due to the decrease in the average ZnO grain size. It can be seen that the relation between varistor voltage and average grain size is opposite.

The nonlinear coefficient (α) decreased in the range of 45.7-35.9 with the increase of the sintering temperature. The sintering temperature has a significant effect on nonlinear properties. The reason why the sintering affects nonlinear properties is suggested as to due to the decrease of barrier height at grain boundaries. When the sintering temperature increases, many ions migrate interior and exterior of the grains. As a result, the electronic states will vary at grain boundaries and lead to any variation in the potential barrier. The leakage current density (J_L) was in the range 7.24-9.49 $\mu A \cdot cm^{-2}$.

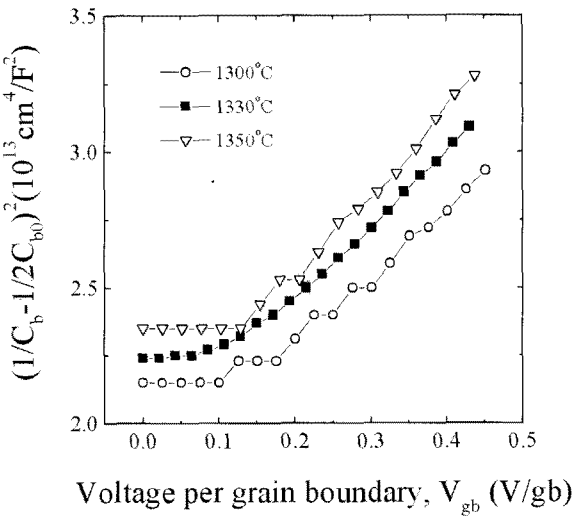

Fig. 4. C-V characteristics of the samples s for different sintering temperatures.

Figure 4 shows the capacitance-voltage of the samples for different sintering temperatures. The variation of capacitance with applied voltage provides a large amount of information such as donor concentration of ZnO grain (N_d), density of interface states (N_t), barrier height (Φ_b), as shown in Table 1. The N_d decreased in the range of $9.06\text{-}7.24 \times 10^{17}$ cm^{-3} with the increase of the sintering temperature. The increase of the depletion layer width (t) is attributed to the decrease of donor concentration. In general, the depletion

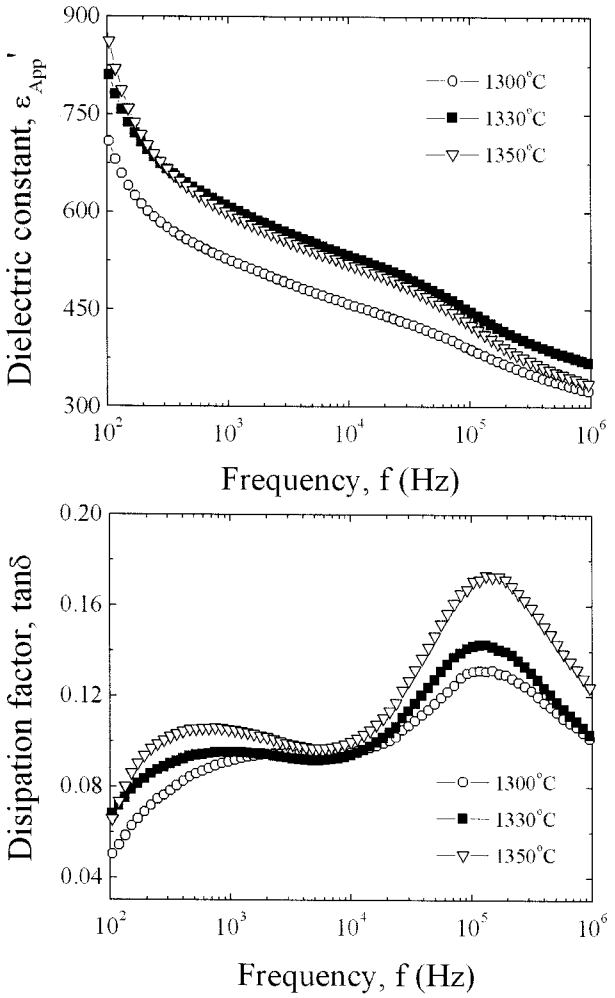

Fig. 5. Dielectric characteristics of the samples for different sintering temperatures.

region extends farther into the side with a lighter doping. The density of interface state decreased from 3.06×10^{12} to 2.54×10^{12} cm^{-2} with the increase of the sintering temperature. This is attributed to the decrease of negatively charged zinc vacancy at grain boundary when the sintering temperature is increased. This decrease may cause the decrease of barrier height in the range of 1.1-0.95 eV. The decrease in the barrier height with the increase of the sintering temperature impaired the nonlinear properties of varistor, as shown in the experimental results.

Figure 5 shows the frequency dependence of dielectric constant (ε_{APP}') and dissipation factor (tanδ) of the samples for different sintering temperatures. The ε_{APP}' is on of dielectric properties of material, which is dependent on frequency. The static dielectric constant is an effect of polarization under a DC condition. When the applied field is a sinusoidal signal, then the polarization of medium under these AC conditions leads to a dielectric constant that is generally different than the static case. The sinusoidally varying field continuously changes magnitude and direction and it tries to line up the dipoles one-way and then the other way. If the field changes too rapidly, then the dipoles cannot follow the field and as a consequence remain randomly oriented[19]. Eventually (as shown in Fig. 5) the

Table 2. Dielectric parameters of the samples for different sintering temperatures.

Sintering temperature (°C)	1300	1330	1350
ε_{APP}' (1 kHz)	529.1	610.3	601.2
tanδ (1 kHz)	0.0910	0.0951	0.1053

ε_{APP}' is gradually decreased for all the samples and is known as the dielectric dispersion phenomena. The ε_{APP}' shows a slightly different behavior with the sintering temperature and is entirely dominated to the average grain size and deletion layer width according to the following equation:

$$\varepsilon_{APP}' = \varepsilon_g \cdot \frac{d}{t} \tag{6}$$

The ε_{APP}' at 1 kHz exhibited relatively low value in the range of 529.1-610.3.

The tanδ represents the energy dissipation in the sample medium as the dipoles are oriented against random collisions one-way and then the other way by the field. This depends on the frictional loss of dipole rotation under AC field and the joule loss by current leakage. As seen in Fig. 2, the tanδ of the samples sintered at 1330 °C and 1350 °C increased when the frequency increased to approximately 1 kHz, and thereafter it decreased to approximately 5.4 kHz. When the frequency increased continuously, the tanδ of all the samples exhibited a peak in the vicinity of 192 kHz. The curve of the tanδ exhibited a complicated behavior. The tanδ at 1 kHz exhibited a high value in the range of 0.0910-0.1053. The detailed dielectric parameters are summarized in Table 2.

4. CONCLUSION

The microstructure, V-I, C-V, and dielectric characteristics of the varistors were investigated at different sintering temperatures. The sintered ceramics are not greatly affected by the sintering temperature due to the high density (5.8 $g\cdot cm^{-3}$) that is close to saturation in the range of the sintering temperature in this study. The average grain size increased from 4.3 to 5.1 μm with the increase of the sintering temperature. As the sintering temperature increased, the breakdown field decreased from 7,531 to 5,882 $V\cdot cm^{-1}$ and the nonlinear coefficient decreased from 46 to 36 with the increase of the sintering temperature. In C-V characteristics, as the sintering temperature increased, the donor density, density of interface states, and barrier height decreased in the range of $(9.06\text{-}7.24)\times10^{17}$ cm^{-3}, $(3.05\text{-}2.56)\times10^{12}$ cm^{-2}, and 1.1-0.95 eV, respectively. The dielectric constant was relatively low in the range of 529.1-610.3, whereas the tanδ was high in the range of 0.0910-0.1053.

ACKNOWLEDGEMENT

This work was supported by Dong-eui University grant (No. 2008AA162).

REFERENCES

[1] L. M. Levinson and H. R. Philipp, Amer. Ceram. Soc. Bull. **65**, 639 (1986).
[2] T. K. Gupta, J. Am. Ceram. Soc. **73**, 1817 (1990).
[3] Y. S. Lee and T. Y. Tseng, J. Am. Ceram. Soc. **75**, 1636 (1992).
[4] A. B. Alles and V. L. Burdick, J. Appl. Phys. **70**, 6883 (1991).
[5] A. B. Alles, R. Puskas, G. Callahan, and V. L. Burdick, J. Am. Ceram. Soc. **76**, 2098 (1993).
[6] Y.-S. Lee, K.-S. Liao, and T.- Y. Tseng, J. Am. Ceram. Soc. 79, 2379 (1996).
[7] C.-W. Nahm, Mater. Lett. **47**, 182 (2001).
[8] C.-W. Nahm and J.-S. Ryu, Mater. Lett. **53**, 110 (2002).
[9] C.-W. Nahm, Mater. Lett. **57**, 1317 (2003).
[10] C.-W. Nahm and B.-C. Shin, Mater. Lett. **57**, 1322 (2003).
[11] C.-W. Nahm, Mater. Lett. **58**, 2252 (2004).
[12] C.-W. Nahm and B.-C. Shin, J. Mater. Sci.: Mater. Electron. **16**, 725 (2005).
[13] C.-W. Nahm, Mater. Lett. **60**, 3394 (2006).
[14] C.-W. Nahm, Trans. Electr. Electron. Mater. **8**, 105 (2007).
[15] C.-W. Nahm, Mater. Lett. **62**, 2900 (2008).
[16] J. C. Wurst and J. A. Nelson, J. Am. Ceram. Soc. **55**, 109 (1972).
[17] M. Mukae, K. Tsuda, and I. Nagasawa, J. Appl. Phys. **50**, 4475 (1979).
[18] L. Hozer, Semiconductor Ceramics: Grain Boundary Effects, Ellis Horwood, (1994), p. 22.
[19] S. O. Kasap, Electronic Materials and Devices, McGraw-Hill, (2002), p. 526.